Measurement and analysis of thermopower and electrical conductivity of an indium antimonide nanowire from a vapor-liquid-solid method

Jae Hun Seol, Arden L. Moore, Sanjoy K. Saha, Feng Zhou, and Li Shi[a)]
Department of Mechanical Engineering, The University of Texas at Austin, Austin, Texas 78712 and Center for Nano and Molecular Science and Technology, Texas Materials Institute, The University of Texas at Austin, Austin, Texas 78712

Qi Laura Ye and Raymond Scheffler
NASA Ames Research Center, Moffett Field, California 94035 and ELORET, 465 S. Mathilda Avenue, Suite 103, Sunnyvale, California 94086

Natalio Mingo and Toshishige Yamada
NASA Ames Research Center, Moffett Field, California 94035

(Received 25 August 2006; accepted 13 November 2006; published online 22 January 2007)

It has been suggested by theoretical calculation that indium antimonide (InSb) nanowires can possess improved thermoelectric properties compared to the corresponding bulk crystal. Here we fabricated a device using electron beam lithography to measure the thermopower and electrical conductivity of an individual InSb nanowire grown using a vapor-liquid-solid method. The comparison between the measurement results and transport simulations reveals that the nanowire was unintentionally degenerately doped with donors. Better control of the impurity doping concentration can improve the thermoelectric properties. © *2007 American Institute of Physics*.
[DOI: 10.1063/1.2430508]

I. INTRODUCTION

Indium antimonide (InSb) is a small band gap semiconductor with high carrier mobility and small effective mass, and is widely used in optical detectors, high-speed electronic devices, and magnetic field sensors. Recent experimental results have shown that bulk InSb is a promising candidate for thermoelectric power generation, with a thermoelectric figure of merit $ZT \equiv S^2\sigma T/\kappa$ of 0.6 at temperature of 673 K,[1] where S is the Seebeck coefficient, σ is the electrical conductivity, κ is the thermal conductivity, and T is the absolute temperature. As to the one dimensional (1D) counterpart, InSb nanowires have attracted great interest both in the study of low-dimensional transport and for practical applications. A theoretical calculation suggested that InSb nanowires with a diameter below 15 nm can have a ZT higher than 1 at room temperature.[2] As a comparison, bismuth telluride alloys have remained the bulk materials with the highest ZT with a value close to 1 at temperature of 300 K. The predicted ZT enhancement in InSb as well as in Bi-based nanowires[3] is attributed to reduction in the lattice thermal conductivity because of diffuse phonon-surface scattering as well as to the enhanced power factor ($S^2\sigma$) of electrons that are confined to one dimension.

Measurement results of thermoelectric properties of individual InSb nanowires have not been reported by others in the literature. In this work, we have fabricated a device using electron beam lithography (EBL) to measure the Seebeck coefficient (or thermopower) and electrical conductivity of an InSb nanowire that was synthesized using a vapor-liquid-solid (VLS) method. We have analyzed the measurement results using transport models of Seebeck coefficient and electrical conductivity. The measurement and analysis are discussed in the following sections.

II. EXPERIMENTAL METHODS

The nanowires were grown on a quartz wafer or a silicone dioxide (SiO_2) coated silicon (100) wafer using the VLS method.[4] After the nanowires were scraped from the wafer with the use of a razor blade, they were dispersed in isopropyl alcohol (IPA). To obtain the Seebeck coefficient and four-probe electrical resistance of the nanowire, we used EBL to fabricate a measurement device shown in Fig. 1. The fabrication of this device consists of two EBL steps. In the first EBL step, large contact pads, electrodes, and alignment marks were patterned on a 1-μm-thick SiO_2 film grown on top of a silicon wafer. After a drop of the nanowire suspen-

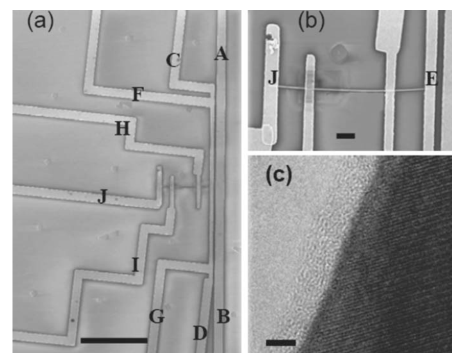

FIG. 1. (a) Scanning electron microscopy (SEM) of the measurement device. Scale bar=10 μm. (b) Enlarged view of the four electrodes on the InSb nanowire. Scale bar=1 μm. (c) Transmission electron microscopy (TEM) image of an InSb nanowire. Scale bar=3 nm.

[a)]Author to whom correspondence should be addressed; electronic mail: lishi@mail.utexas.edu

 © 2007 American Institute of Physics

Downloaded 23 Jan 2007 to 128.114.63.229. Redistribution subject to AIP license or copyright, see http://jap.aip.org/jap/copyright.jsp

sion was dried on the wafer, we used scanning electron micposcopy (SEM) to locate a nanowire deposited on the wafer and measure its position relative to the alignment marks made during the first EBL step. During the second EBL step, fine gold (Au) electrodes were patterned on the nanowire together with a heater line and an adjacent resistance thermometer line patterned on the nanowire. To improve the electrical contact between the nanowire and the metal electrodes, a 3 min immersion of the device in a solution of 23.7% of $(NH_4)_2S$ in water was used to passivate the surface of the nanowire segments exposed through windows opened in the EBL resist, i.e., polymethylmethacrylate (PMMA), after PMMA was developed and before the metal was evaporated on the wafer and contact the exposed nanowire segments. Solutions based on $(NH_4)_2S_x$ have been commonly used for passivating the surface of III-IV compounds.[5–7] During the passivation, the native oxide layer on the InSb nanowire surface was removed and the dangling bonds on the nanowire surface were terminated with a monolayer of sulfur atoms that prevented the formation of a native oxide layer on the nanowire.

As shown in Fig. 1(a), A-B is the heater and C-D is the thermometer. When the heater line was heated by a direct current (I), the four-probe resistance of the (R) thermometer between F and G was measured using a 500 nA sinusoidal excitation current and a lock-in amplifier. The average temperature rise ($\Delta\bar{T}$) of the thermometer line was obtained from the measured resistance increase (ΔR) of the thermometer line at different heating current levels according to $\Delta\bar{T}=\Delta R/(dR/dT)$, where dR/dT was obtained by measuring R at different base temperatures (T) of the sample stage in an evacuated cryostat. During the measurement, $\Delta\bar{T}$ was kept below 4 and 7 K at temperatures below and above 200 K, respectively. The thermovoltage (ΔV) between J and E in Fig. 1(b) was measured and used to calculate the Seebeck coefficient as $S=\Delta V/\Delta\bar{T}$. Because the Seebeck coefficient of Au is only 1.94 μV/K at temperature of 300 K and much smaller than that of InSb,[8] the thermovoltage in the Au electrodes was ignored.

A commercial software (ANSYS) was used to obtain the temperature distribution on the device surface when a current passes the heater line of the device. As shown in Fig. 2, the temperature rise ΔT_E of point E in Fig. 1(b), which was the contact point between the nanowire and the thermometer line, was found to be 16.5% higher than $\Delta\bar{T}$. Three additional electrodes contacted the nanowire. The temperature rise ΔT_J at the contact between the nanowire and electrode J in Fig. 1(b) was found in the thermal simulation to be about 4.8% of $\Delta\bar{T}$. Thus, the temperature difference $\Delta T_{E\text{-}J}$ between the two contact points was estimated to be about 12% higher than $\Delta\bar{T}$. This simulation result suggests that the as-obtained Seebeck coefficient $S=\Delta V/\Delta\bar{T}$ could be about 12% higher than the actual S value of $\Delta V/\Delta T_{E\text{-}J}$.

For the sample shown in Fig. 1, the distance between the two inner electrodes (H and J) was 3.574 μm and the average diameter of the InSb nanowire was 41.5 nm. For measuring the four probe electrical resistance, the two outer electrodes (C and J) were used as the current source and drain, and the two inner electrodes (H and I) were used as the voltage probes.

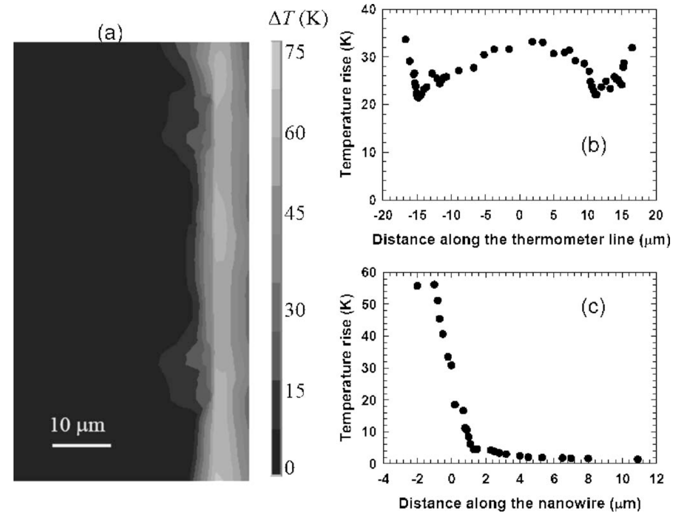

FIG. 2. (a) Calculated surface temperature rise (ΔT) of the device shown in Fig. 1(a) when a current passes through the heater line. The dimension of the thermal image is 40 μm wide and 80 μm long. Point E in Fig. 1(b) is located at 40 μm below the top edge and 5 μm from the right edge. (b) Temperature rise along the thermometer line. Point E in Fig. 1(b) is located at 0 μm. (c) Temperature rise along the nanowire. Points E and J in Fig. 1(b) are located at 0 and 11 μm, respectively.

III. MEASUREMENT RESULTS AND ANALYSIS

Shown in Fig. 3, the as-measured Seebeck coefficient of the InSb nanowire was found to be approximately an order of magnitude smaller than the bulk values reported in literature for doping concentrations of 2×10^{14} and 7×10^{15} cm^{-3}, respectively.[1,9]

Figure 4 shows the electrical conductivity obtained from the measured four-terminal electrical resistance as a function of temperature. The electrical conductivity of this nanowire was found to show much weaker temperature dependence

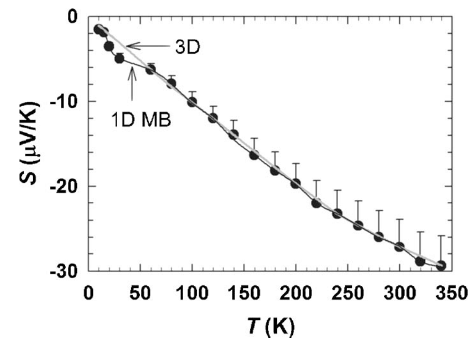

FIG. 3. The measurement results of Seebeck coefficient (S) of the InSb nanowire as a function of temperature (T). The filled circles are the as-measured data ($S=\Delta V/\Delta\bar{T}$) and the upper bounds of the error bars are the corrected ones ($S=\Delta V/\Delta T_{E\text{-}J}$) based on the temperature measurement error estimated by the thermal simulation. The calculation results based on the 1D MB (black line) and 3D (gray line) DOS were made to fit with the as-measured data by adjusting the corresponding Fermi energy values at different temperatures, and cannot be distinguished from each other in many areas of the plot.

Downloaded 23 Jan 2007 to 128.114.63.229. Redistribution subject to AIP license or copyright, see http://jap.aip.org/jap/copyright.jsp

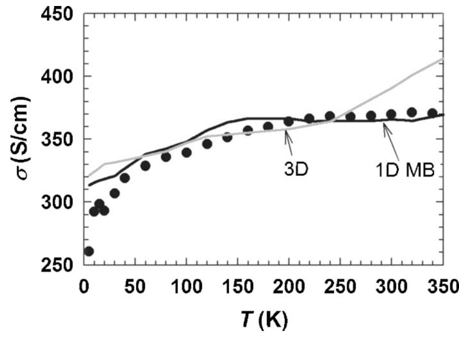

FIG. 4. The measurement results (filled circles) of the electrical conductivity of the InSb nanowire as a function of temperature. The black line and the gray line are the calculation results of the 1D MB and 3D models, respectively.

and be 33%–125% larger (depending on temperature) than the bulk values reported in the literature for a doping concentration of 1.7×10^{16} cm^{-3}.[10]

The power factor, $S^2\sigma$, was obtained from the measured S and σ values, as shown in Fig. 5 as a function of temperature. The power factor is two orders of magnitude smaller than that of a bulk crystal with an impurity concentration of 2×10^{14} cm^{-3}.[1]

We have compared our measurement results with those reported in the literature for other nanowire systems. Heremans *et al.* reported a weak temperature dependence of electrical conductance in a nanocomposite consisting of 10 nm diameter Sb nanowires in the highly degenerate phase,[11] where the carrier concentration was relatively temperature independent. This behavior was attributed to the increasing relative importance of impurity scattering and surface scattering over phonon scattering, which shows much stronger temperature dependence than impurity and surface scattering. Stronger temperature dependence was observed in other nanowire samples wider than 10 nm diameter reflecting the increasing dominance of phonon scattering at higher temperature. In addition, Lin *et al.* reported the carrier mobility and electrical conductance for an array of Te-doped Bi nanowires with 40 nm diameter.[12] Their results showed decreasing electrical conductance for increasing temperature and for decreasing Te-doping concentration. The results reveal the roles of phonon scattering and doping on electron transport in highly degenerate nanowires.

In order to gain a better understanding of the observed

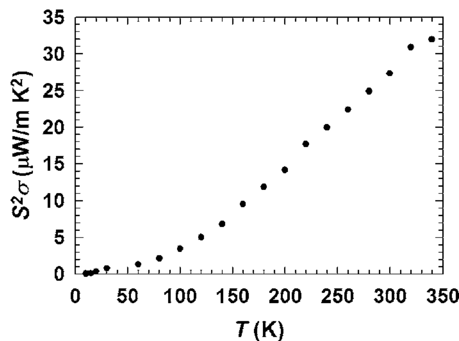

FIG. 5. The thermoelectric power factor $S^2\sigma$ of the InSb nanowire as a function of temperature.

electrical conductivity and Seebeck coefficient of the InSb nanowire, theoretical models of these transport coefficients were used to analyze the measurement results. Only the carriers at the Γ valley of InSb were considered in the simulation because the band gap values at the L and X valleys are much higher than at the Γ valley. For n-type InSb, the ratio of electron mobility to hole mobility is approximately 100,[13] and the ratio of electron concentration to hole concentration in the InSb nanowire was found to be many orders of magnitudes larger. As such, the hole contributions to the Seebeck coefficient and electrical conductivity were ignored and only the electron contributions were taken into account. The Seebeck coefficient of electrons in the conduction band is calculated as[14]

$$S = \frac{1}{eT}\left\{ E_F - \frac{\int_0^\infty g(E)\tau_e E^2[\partial f_0(E)/\partial E]dE}{\int_0^\infty g(E)\tau_e E[\partial f_0(E)/\partial E]dE} \right\}, \quad (1)$$

where e is the electron charge, T is the absolute temperature, E_F is the Fermi level measured from the conduction band edge (E_C), $g(E)$ is the density of states (DOS) of electrons, τ_e is the electron scattering mean free time, and $f_0(E) = 1/\{\exp[(E-E_F)/k_BT]+1\}$ is the Fermi-Dirac distribution function with k_B being the Boltzmann constant. The mean free time is assumed to depend on the electron energy according to $\tau_e=\tau_0 E^{r_e}$, where τ_0 and r_e are two constants. For the InSb nanowire, τ_e was found to be mainly limited by the boundary scattering mean free time, $\tau_{\text{boundary}}=L_{\text{boundary}}/v$, where L_{boundary} is the boundary scattering mean free path, which is assumed to be independent of energy and temperature, and v is the electron velocity and is proportional to $E^{1/2}$. Hence, we have used a r_e value of -0.5.

Due to size confinement in the radial direction of the 41.5 nm diameter InSb nanowire, the energy separation between two adjacent electron subbands is on the order of the thermal broadening (k_BT) of the Fermi-Dirac function near room temperature. Hence, the following DOS with multiple 1D subbands is more adequate than a single 1D subband model[15] for calculating the transport coefficients,

$$g(E)_{1\text{D}}dE = \frac{4}{\pi^2 d^2}\left(\frac{2m_e^*}{\hbar^2}\right)^{1/2}\sum_i \left[\frac{n_i H(E-E_i)}{(E-E_i)^{1/2}}\right]dE, \quad (2)$$

where d is the diameter of the nanowire, m_e^* is the electron effective mass, $\hbar$ is Planck's constant, the degeneracy factor n_{i} equals 1 for $i=1$, 3, and 7 and equals 2 for other i values in the range between 2 and 10, $H(E-E_i)$ is the Heaviside function and takes the value of 0 and 1 when E is less and greater than E_i, respectively, and $E_i=M_i(\pi^2\hbar^2)/2m_e^* d^2$ with M_i=2, 5, 8, 10, 13, 17, 18, 20, 25, and 26, respectively, for $i=1,2,\ldots,10$.

At different temperatures, E_F was adjusted in order to best fit the measurement data of Seebeck coefficient using Eq. (1). The obtained E_F as a function of temperature was used to determine the carrier concentration n at different temperatures according to

Downloaded 23 Jan 2007 to 128.114.63.229. Redistribution subject to AIP license or copyright, see http://jap.aip.org/jap/copyright.jsp

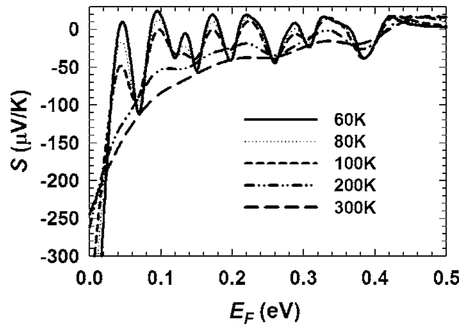

FIG. 6. Seebeck coefficient (S) vs Fermi level (E_F) for the MB DOS at different temperatures.

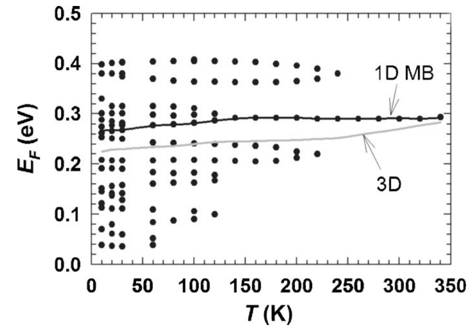

FIG. 7. Fermi levels (E_F) used for the 1D MB (black line) and 3D (gray line) models. Solid circles represent possible values of E_F that can yield the as-measured S values at different temperatures using the 1D MB model.

$$n(T) = \int_0^\infty g(E) f_0(E) dE. \tag{3}$$

The electrical conductivity was calculated according to

$$\sigma = ne\mu, \tag{4}$$

where μ is the carrier mobility. Matthiessen's rule was used to obtain $\mu^{-1} = \mu_{\text{bulk}}^{-1} + \mu_{\text{boundary}}^{-1}$, where μ_{bulk} and μ_{boundary} are the mobility for bulk InSb crystals and that due to additional boundary scattering in the nanowire. The bulk mobility μ_{bulk} is taken from reported electron mobility data for single-crystal InSb samples with varying doping concentrations ranging from being very pure to degenerately doped.[16] This term accounts for both phonon and impurity scattering events. For modeling of nanowires, the electron mean free path due to boundary scattering L_{boundary}, which is assumed to be independent of temperature, was adjusted in order to obtain the μ_{boundary} that can best fit with our experimental conductivity data.

In addition to the 1D multisubband (MB) DOS in Eq. (2), we have performed the same calculation using a three dimensional (3D) DOS. For the 3D DOS, the equations for Seebeck coefficient and carrier concentration are reduced to

$$S_{3D} = \frac{k_B}{e}\left\{ \eta - \frac{[r_e + (5/2)]F_{r_e+3/2}}{[r_e + (3/2)]F_{r_e+1/2}} \right\}; \quad \eta = \frac{E_F}{k_B T}, \tag{5}$$

and

$$n_{3D}(T) = \frac{(2m_e^* k_B T)^{3/2}}{2\pi^2 \hbar^3} F_{1/2}, \tag{6}$$

where $F_m(\eta) = \int_0^\infty \xi^m d\xi / [e^{(\xi-\eta)} + 1]$ is the Fermi-Dirac integral of order m.

Due to the multiple sharp peaks in the 1D MB DOS, the determination of E_F to match the Seebeck coefficient data was not as straightforward for the MB model as for the 3D model. For Fermi level close to each of these peaks in the 1D MB DOS, a small change in the Fermi energy can result in a large change in the Seebeck coefficient,[17] as illustrated in Fig. 6 as the large modulation in Seebeck coefficient with changes in the Fermi energy. Similar modulation of Seebeck coefficient with the Fermi level due to Coulomb blockade has been seen experimentally in metallic carbon nanotubes.[18] The modulation is more significant at low temperatures than at high temperatures, because increased thermal broadening of the Fermi-Dirac function with temperature reduces the influence of the peaks in the DOS on the Seebeck coefficient. At temperatures below 250 K, the modulation in Seebeck coefficient yields multiple values of E_F that may result in the measured Seebeck coefficient. By determining all possible values of E_F at different temperatures and examining the magnitude and temperature dependence of the carrier concentration and electrical conductivity that correspond to each possible E_F value, one may eliminate the majority of the possible solutions at each temperature and obtain a reasonable E_F versus temperature trend. For the MB model, all possible values of E_F at the measured temperatures are shown in Fig. 7, with the values of E_F used in the different models of DOS indicated by the trend lines. The calculated Seebeck coefficient based on the E_F values is shown in Fig. 3 together with the measurement results.

The E_F values in Fig. 7 determined by the MB model reside in the seventh and eighth electron subbands. In nondegenerate n-type semiconductors, the Fermi level usually decreases with increasing temperature. The high E_F values and the trend of a slight increase of E_F with temperature suggest that the nanowire is degenerately doped. As shown in Fig. 8, the obtained carrier concentrations calculated based on the E_F values is well beyond the intrinsic carrier concentration in bulk InSb of 2×10^{16} cm^{-3} at a temperature of 300 K. The weak temperature dependence of the carrier concentration also suggests a highly degenerate behavior. The nanowire could have been doped with possibly Te, a known shallow donor for InSb with 0.6 meV ionization energy,[19] taking into account the InSb band gap of 0.24 eV at 0 K and

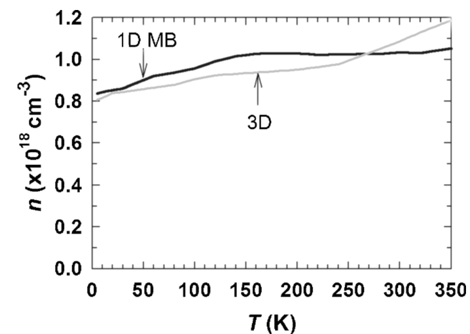

FIG. 8. Calculated carrier concentrations as a function of temperature for the 1D MB (black line) and 3D (gray line) models.

Downloaded 23 Jan 2007 to 128.114.63.229. Redistribution subject to AIP license or copyright, see http://jap.aip.org/jap/copyright.jsp

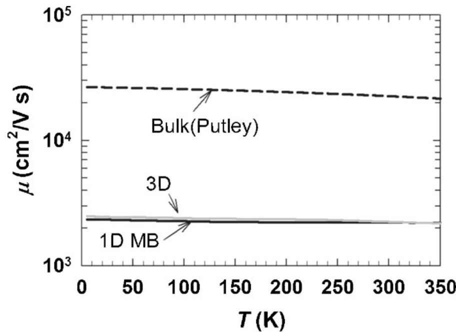

FIG. 9. Mobility as a function of temperature. The dashed line is the bulk mobility reported by Putley (Ref. 16) for electron concentration of 1.15 $\times 10^{18}$ cm^{-3}. The gray and black solid lines are the electron mobility used in the 3D and 1D MB models, respectively, for fitting the measured electrical conductivity of the nanowire.

0.17 eV at 300 K, respectively. We suspect that the impurity was incorporated in the InSb powders, rated at 99.999% purity, that were used as the source materials for VLS growth of the nanowires.

Figure 9 shows the bulk mobility reported in the literature[16] for an electron concentration of 1.15 $\times 10^{18}$ cm^{-3} that is similar to that found for the nanowire together with the mobility used in the different DOS models for fitting the measured electrical conductivity of the nanowire. The electrical conductivity data calculated using the MB DOS show better agreement with the measurement results than the 3D model, as shown in Fig. 4. For the 3D and MB models, L_{boundary} was 52 and 53 nm, respectively, comparable to the measured nanowire diameter of 41.5 nm. As a comparison, the scattering mean free paths (L_{bulk}) of electrons due to impurity and phonon scatterings were 468 and 485 nm at 300 K for the 3D and MB models, respectively. Hence, the electron mean free path is determined by diffuse surface scattering of electrons. Using a simple unscreened surface roughness scattering model, one can estimate the specularity (p) of the nanowire surface that depends on the wavelength (λ) of the incident particles according to $p(\lambda) \approx \exp(-16\pi^3 r^2/\lambda^2)$.[20,21] The specular and diffuse surface scattering cases correspond to a p value of 1 and 0, respectively. The surface roughness r of the nanowire was found by transmission electron microscopy (TEM) to be in the range of 0.5–1 nm, as shown in Fig. 1. The Fermi wavelength is estimated to be $\lambda_F = 2\pi\hbar/\sqrt{2m_e E_F} \sim 20$ nm at 300 K based on the Fermi level determined for the 1D MB and 3D models, respectively. Based on these values, p takes the values in the range of 0.26–0.72 and 0.29–0.73 for the 1D MB and 3D models, respectively. Hence, electron scattering by the nanowire surface is partially specular and partially diffuse for both models, and the equivalent L_{boundary} can range from one to several times the nanowire diameter. Combined with a weak temperature dependence of the carrier concentration, the increasing relative importance of surface scattering over phonon scattering in the nanowire could have resulted in the weak temperature dependence of the nanowire electrical conductivity shown in Fig. 4.

The calculation results offer some insight into the effect of unintentional doping and surface roughness scattering on the electron transport. Further, it reveals the large variation of Seebeck coefficient with Fermi level in a 1D MB system, and stress the importance of carefully tuning the Fermi level by controlling the doping concentration in order to obtain an optimized power factor in nanowires.

However, many of the properties such as the effective mass and mobility of Te-doped InSb used in the calculation were taken from bulk values published in literature. These parameters for bulk InSb may be different from those for nanowires. Additionally, it should be noted that the actual diameter for electron transport within the nanowire should be smaller than that measured by SEM due to the presence of the native oxide layer. Moreover, the analysis does not take into the effects of surface depletion due to trapped charge states.[22,23] It also ignores the possible existence of Luttinger liquid-like strong electron-electron interaction,[24] features of which were found in the current-voltage characteristics of the InSb nanowire sample reported here.[25]

IV. CONCLUSION

The measurements reveal low Seebeck coefficient and high electrical conductivity of an InSb nanowire grown using a VLS method compared to those for pure bulk InSb crystals. The measurement results agree reasonably well with the multiple subband model of electron transport in a *n*-type degenerately doped InSb nanowire, where the electron scattering mean free path is close to the nanowire diameter due to partially diffuse surface roughness scattering. The calculation further reveals large modulation of Seebeck coefficient with the Fermi energy and stresses the importance of tuning the Fermi level by controlling the impurity doping concentration in order to optimize the power factor of nanowires.

ACKNOWLEDGMENTS

This work is supported by NASA under Contract No. NNA05BE36C to ELORET. The authors at Austin are supported in part by Office of Naval Research Contract No. N00014-04-1-0532 (Program Manager: Dr. Mihal E. Gross) and the DARPA Advanced Processing and Prototyping Center.

[1]S. Yamaguchi, T. Matsumoto, J. Yamazaki, N. Kaiwa, and A. Yamamoto, Appl. Phys. Lett. **87**, 201902 (2005).
[2]N. Mingo, Appl. Phys. Lett. **84**, 2652 (2004); **88**, 149902(E) (2006).
[3]X. Sun, Z. Zhang, and M. S. Dresselhaus, Appl. Phys. Lett. **74**, 4005 (1999).
[4]Q. Ye, T. Yamada, H. Liu, R. H. Scheffler, N. Mingo, and R. L. Leverenz, Mater. Res. Soc. Symp. Proc. **940E**, P7.5 (2006).
[5]A. Gin, Y. Wei, A. Hood, A. Bajowala, V. Yazdanpanah, M. Razeghi, and M. Tidrow, Appl. Phys. Lett. **84**, 2037 (2004).
[6]M. Jeng, H. Wang, L. Chang, and R. Lin, Jpn. J. Appl. Phys., Part 1 **40**, 562 (2001).
[7]H. Oigawa, J. Fan, Y. Nannichi, H. Sugahara, and M. Oshima, Jpn. J. Appl. Phys., Part 1 **30**, 322 (1991).
[8]D. M. Rowe, *CRC Handbook of Thermoelectrics* (CRC, Boca Raton, FL, 1995), p. 390, Chap. 32.
[9]H. P. R. Frederikse and E. V. Mielczarek, Phys. Rev. **99**, 1889 (1955).
[10]M. Tanenbaum and J. P. Maita, Phys. Rev. **91**, 1009 (1953).
[11]J. Heremans, C. Thrush, Y. Lin, S. Cronin, and M. Dresselhaus, Phys. Rev. B **63**, 085406 (2001).
[12]Y. Lin, S. Cronin, J. Ying, M. Dresselhaus, and J. P. Heremans, Appl. Phys. Lett. **76**, 3944 (2000).
[13]Y. J. Jung, M. K. Park, S. I. Tae, K. H. Lee, and H. Lee, J. Appl. Phys. **69**,

Downloaded 23 Jan 2007 to 128.114.63.229. Redistribution subject to AIP license or copyright, see http://jap.aip.org/jap/copyright.jsp

3109 (1999).
[14] G. S. Nolas, J. Sharp, and H. J. Goldsmid, *Thermoelectrics* (Springer, New York, 2001).
[15] Y. Lin, X. Sun, and M. Dresselhaus, Phys. Rev. B **62**, 4610 (2000).
[16] E. H. Putley, Proc. Phys. Soc. London **73**, 280 (1959).
[17] M. J. Kearney and P. N. Butcher, J. Phys. C **19**, 5429 (1986).
[18] J. Small, K. Perez, and P. Kim, Phys. Rev. Lett. **91**, 256801 (2003).
[19] C. L. Littler and D. G. Seiler, J. Appl. Phys. **60**, 261 (1986).
[20] J. M. Ziman, *Electrons and Phonons* (Clarendon, Oxford, 1960).
[21] T. Yamada, H. Miyata, J. R. Zhou, and D. K. Ferry, Phys. Rev. B **49**, 1875 (1994).
[22] J. Bardeen, Phys. Rev. **71**, 717 (1947).
[23] I. Kimukin, M. Saif Islam, and R. Williams, Nanotechnology **17**, S240 (2006).
[24] S. V. Zaitsev-Zotov, Y. A. Kumzerov, Y. A. Firsov, and P. Monceau, J. Phys.: Condens. Matter **12**, L303 (2000).
[25] F. Zhou, J. H. Seol, A. L. Moore, L. Shi, Q. L. Ye, and R. Scheffler, J. Phys.: Condens. Matter **18**, 9651 (2006).

Downloaded 23 Jan 2007 to 128.114.63.229. Redistribution subject to AIP license or copyright, see http://jap.aip.org/jap/copyright.jsp